Solar Energy, Volume 197, February 2020, pp. 105-110
DOI: 10.1016/j.solener.2019.12.050

Numerical simulation of heat distribution in RGO-contacted perovskite solar cells using COMSOL

Soma Zandi[a], Prateek Saxena[b], Nima E. Gorji[c,*]

[a] *Department of Electrical Engineering, School of Engineering, University of Kurdistan, Sanandaj, Iran*
[b] *Sustainable Manufacturing Systems Centre, School of Aerospace, Transport and Manufacturing, Cranfield University, Bedfordshire, UK*
[c] *Optoelectronics Research Group, Faculty of Electrical and Electronics Engineering, Ton Duc Thang University, Ho Chi Minh City, VietNam*

Abstract

A 3D simulation of optical photogenreation, electrical characteristics, and thermal/heat distribution across the structure of a perovskite solar cell with a reduced graphene oxide (RGO) contact is presented. COMSOL Multiphysics package has been used to solve the coupled optical-electrical-thermal modules for this hybrid cell where the RGO added as the bottom electrode instead of a conventional metallic contact to enhance the heat dissipation towards a higher device stability. The Wave Optic module, Semiconductor module, and Heat Transfer in Solid module were coupled and solved for the proper input parameter values taken from relevant literature. The optical photogeneration, current-voltage characteristics, electric-field and the thermal maps of the cell are presented. The RGO contact doesn't significantly impact on the optical and electrical output of the cell, but it accelerates the heat dissipation. The heat is mainly generated across the cell from the light absorption, Shockley-Read-Hall non-radiative recombination, and Joule heating. Compared to the cell with the Au electrode, the RGO contacted cell is showing a minimized heat accumulation and gradient at the bottom junction of the RGO/Spiro interface which promises a thermal stability of the cell. The nan-radiative and joule heat distribution also show a moderated density for the RGO contacted cell which are assigned to the high heat conductivity of the RGO layer compared to traditional metallic electrodes. Our simulations results are of the rarely presented thermal simulations for such devices and prove the superiority of graphene over plane metallic contacts for heat dissipation and thermodynamic aspect of a solar cell.

Keywords: Perovskite, Graphene, RGO, Solar cells, COMSOL, Simulation, Heat distribution.

1. Introduction

Graphene with covalent sp^2 bonds, and its derivative oxides including graphene oxide (GO) and reduced graphene oxide (RGO) has been introduced as a promising material for the back contact of solar cells [1, 2, 3]. The high electrical and thermal conductivity, transparency, thin thickness, and flexibility makes the graphene derivatives the ideal candidates for perovskite photovoltaics. The two dimensional graphene sheet has an excellent thermal conductivity in the range of 3600-5400 W/m.K at room temperature. Such a high thermal/electrical conductivity is assigned to it's extraordinary high electron mobility of 15,000 $cm^2/(V.s)$ [4]. Graphene has been used as the electrode in perovskite solar cells to foster the heat dissipation and reducing the perovskite's decomposition rate [5] or ion electroimmigration at high temperature [6]. The RGO layer can protect the perovskite layer from moisture ingression which enhances the thermal and electrical stability of the cell by preventing the PbI_2 defective surface layer. RGO layer can also enhance the heat dissipation to keep the temperature of the cell below 80 °C which is essential for the performance stability over time. Simulation analysis of heat dissipation in graphene contacted perovskite solar cells using the 1D platforms (SCAPS-1D, AMPS-1D, etc.) may not be feasible (or valid), because, solar cells are basically 3D structures and graphene is a 2D or 3D material [1, 7]. Therefore, other platforms such as TCAD-Silvaco or COMSOL multiphysics are suitable for 3D simulation analysis of graphene contacted perovskite solar cells [8, 9]. These 3D simulation packages are capable of solving the coupled optical-electrical-thermal (OET) problems with valid meshing boundary conditions and proper concept physics. Nevertheless, COMSOL was used mostly to map the carrier generation profile, hole and electron concentration profile or optical analysis of solar cells and (to our best of knowledge) no comprehensive simulation were presented in literature on coupled OET problems for heat and temperature mapping in perovskite cells, especially with a graphene contact. Most of such analysis were developed in semi-classical modeling approaches [10, 11]. There is almost no such 3D simulation on graphene contacted solar cells not for thermal mapping nor on heat distribution

* *Email address:* Corresponding author: nimaegorji@tdtu.edu.vn (Nima E. Gorji)

Published by Elsevier. This is the Author Accepted Manuscript issued with: Creative Commons Attribution Non-Commercial No Derivatives License (CC:BY:NC:ND 4.0).
The final published version (version of record) is available online at DOI:10.1016/j.solener.2019.12.050. Please refer to any applicable publisher terms of use.

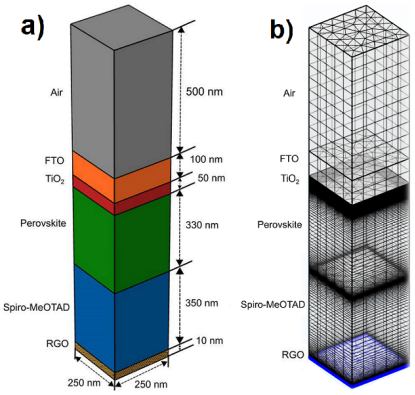


Figure 1: a. The architecture of the RGO-contacted perovskite solar cell in 3D, b. the meshed structure.

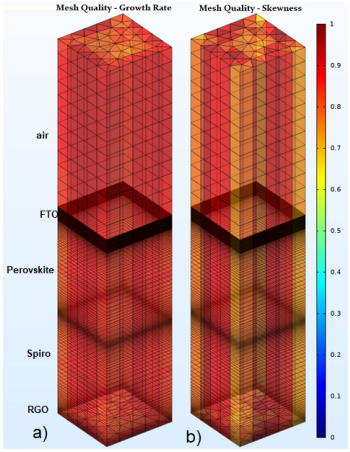


Figure 2: a) The mesh quality created for a) growth rate and b) sknewness.

analysis or heat dissipation in 3D environment. However, the *heat transfer module* in COMSOL enables mapping the heat and temperature across the cell and investigating the contribution of graphene thermal properties to device stability by taking into account the heat generating sources [12, 13]. The Heat Transfer module in COMSOL Multiphysics allows modeling the very high aspect ratio components using the highly conductive layer features such as graphene layer. For such a feature, the heat transfer equation is solved only in the tangential surface plane thus removing the need to use a very fine mesh on the high aspect ratio layers. In turn, the required memory and time for computation is reduced significantly. Paletti et al. have shown that Graphene organic solar cells can be more efficient compared to ITO contacted counterpart if the graphene's series resistance is minimized, and it's work function is optimized (e.g. a doped graphene or RGO) [14].

In this paper, we investigate the optical, electrical and thermal behavior of RGO-contacted perovskite cells using the coupled modules in COMSOL multiphysics package. In particular, we present our 3D simulations of the optical generation rate, current-voltage characteristics, electric field distribution, heat flux and temperature distribution across the cell especially at the RGO/spiro junction. It was found that solar cells with RGO electrode can outperform the others in low thermal degradation rate since the heat flux and temperature distribution at the RGO/Spiro junction is significantly lower than the Au contacted cells. We have provided a coupled model of optical, electrical and thermal models for this 3D system which suits perfectly the 2D nature of a solar cell and the 3D nature of graphene (RGO) electrode.

2. Simulation and Modeling

The thermal conduction in our graphene-contacted perovskite solar cell is simulated using COMSOL software package which numerically solves the partial differential equations in order to investigate the thermal transport in this hybrid structure made of graphene nanostructure and perovskite organic-inorganic layer. The 3D simulations of the optical generation, electric field distribution, recombination rate, current-voltage characteristics, thermal and heat distribution maps are all performed by means of the optical, electromagnetic tool and thermal modules in COMSOL Multiphysics package [15]. The generation rate is calculated by the Wave Optics Module, the electric-field and SRH recombination are calculated using the Electrical Module by inserting the results of the optical module (generation rate, G_{tot}) into Semiconductor Module, and the thermal simulation is performed by "Heat Transfer in Solids" module by loading the heat source with a constant power of 100 mW/cm^2. The sample is cooled down by environment air convection (293.15 K) from top and bottom surfaces. Predefined settings are available for solar and ambient radiation, where the surface absorptivity for short wavelengths (the solar spectral band) may differ from the surface emissivity for the longer wavelengths (the ambient spectral band). According to Thermodynamic laws, the heat moves from higher to lower temperature region when a difference in temperature is there. Heat conduction in semiconductors and metals takes place by electrons carrying heat and in other solids by molecular motion in which crystals take the form of lattice vibrations known as phonons. Heat flux is proportional to temperature gradient. In Graphene, the heat mostly propagates through conduction due to acoustic phonons or atomic vibrations and thus if graphene is used as an electrode, the heat conduction is accelerated to dissipate to the ambient via conduction or by spontaneous transfer of thermal energy from graphene to air. In COMSOL, one can specify the power of the heat source and the thermal conductivity of graphene or RGO.

2.1. Model Geometry

We have previously presented our COMSOL 3D simulations for a conventional perovskite solar cell with Au

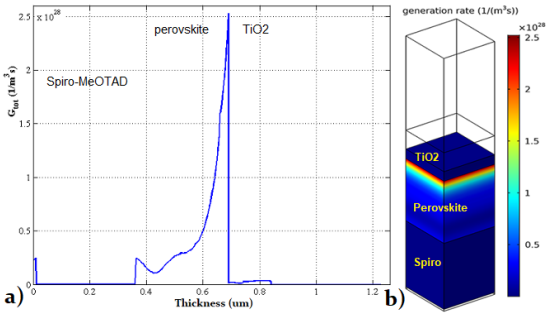


Figure 3: a. the generation rate (G_{tot}) of the RGO-contacted perovskite solar cell in 1D, b. and in 3D.

	FTO	TiO2	Perovskite	Spiro-MeOTAD	RGO contact
N_A (cm^3)	…	…	3×10^{15}	2×10^{18}	…
N_D (cm^3)	2×10^{19}	5×10^{18}	…	…	…
K [W/m.K]	31	4.8	0.5	0.49	1000-2000
ρ [kg/m^3]	5560	3900	4000	4128	1900
C_p [J/kg.K]	343	683	258	262	2000-3000
h [$W/(m^2K)$]	3.1×10^8	9.6×10^7	1.5×10^6	1.4×10^6	$1\text{-}100*10^9$

Table 1: The parameter values of the layers including the electrical and thermal properties of RGO layer [20, 21]

metallic contact (33 nm). Keeping the same cell structure, we just replaced this metallic contact with RGO (10 nm) electrode. This simple change allows us to compare the simulation results of the two conventional and hybrid structure in terms of heat flux and temperature gradient across the cell. The structure of the proposed perovskite solar cell with RGO contact can be found in different literature such as in Ref. [16, 10]. The device structure is shown in the fig. 1a. To simplify the designing process, the thickness of all the layers were taken from our previous work Ref. [17] and only graphene was added instead of Au. This was suggested in several papers for FEM and COMSOL analysis of graphene layer on electronic device structures [18, 19]. According to COMSOL guidebook, air must be added to the surface of the top or bottom of the cell. AM1.5G was used as the input power of the plan wave (300-1000 nm), with normal incident angle only [15]. We assume the cells are initially at room temperature. Most materials properties are selected from COMSOL library but the RGO's optical and thermal properties are manually added from literature [20, 21]. The proper values of refractive index, extinction coefficient of the perovskite layers were taken from literature; For FTO layer from Ref. [22] for Spiro-OMeTAD, perovskite and TiO_2 layers from [4, 10], and RGO layer from Ref. [23]. for thermal conductivity, heat coefficient and density of RGO layer are extracted from literature for a reasonable range some of which are given in Table 1.

2.2. Mesh Structure

A user-controlled mesh is defined for the entire geometry, as shown in 2. Each domain separately meshes with maximum and minimum element size of 52.2 nm and 2.24 nm, respectively. The maximum element growth rate is set to 1.35 with a curvature factor of 0.3. A free triangular mesh is defined for the surface shared by FTO and TiO_2 layers. The tessellation mode is set to automatic. The faces are meshed using a swept meshing sequence with the face meshing method defined as quadrilateral. The TiO_2 layer requires to mesh finely; thus, the number of mesh elements on the face of TiO_2 is set to be 100. For the perovskite layer, the sweep distribution type is defined with 50 elements onto one face with element ratio as 0.1. A symmetric distribution is selected to follow the same distribution pattern on all the faces of the perovskite layer. Same meshing method is extended to Spiro-MeOTAD layer. The RGO layer being the thinnest of all, the distribution of sweep mesh elements on the face is fixed and set to 5 elements on each face. To ensure the mesh quality, quality metrics are chosen. A quality measure can be defined based on skewness, maximum angle, volume versus circumradius, volume versus length, condition number, and growth rate. For the current work, the quality measure is skewness of mesh elements and growth rate. The mesh quality is shown in Fig. 2. Skewness is the most popular and reliable quality measure for the mesh elements used in current work. This quality measure highlights the elements on the basis of their angular skewness. Elements with deviations from ideal mesh (in terms of larger or smaller angles) are penalized. A skewness of 1 is a representative of the best possible mesh, and 0 is indicative of the degenerated mesh element.

Growth rate quality measure compares the size of each mesh element with the neighboring elements in all directions. A growth rate of 1 indicates that the mesh elements in a particular domain are constant in size. A lower value of growth rate indicates that the mesh elements change from one another in the surrounding regions. Thus on the basis of the selected two quality measures, the mesh is found to be acceptable for the current analysis.

3. Physics and the Simulation Results

The most basic use of COMSOL for photovoltaic simulation requires coupling both Semiconductor and Wave Optics modules. Although the heat is transferred by conduction between the layers in the cell, the heat dissipates to ambient air from top FTO electrode or bottom RGO contact via convection. The transient state is neglected here because it takes a relatively short time to reach the steady-state where the temperature is almost stationary at any given point in the cell for a set of given boundary conditions [24]. We define the physics of the study and run the simulations for the optical simulation in Frequency domain analysis and for the electrical and thermal simulations in stationary mode. Solutions from the first study are then used as initial conditions for the second

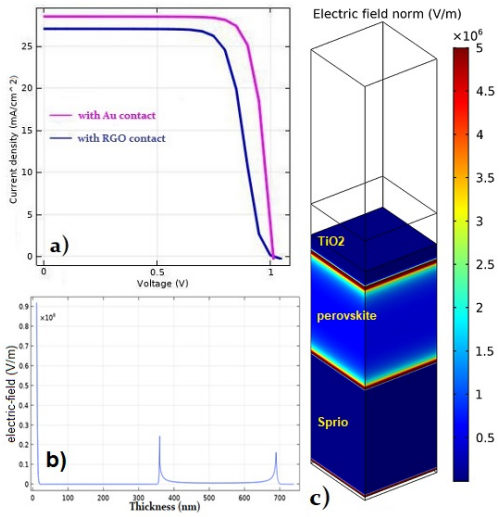


Figure 4: a) the current-voltage characteristics of the perovskite cell with RGO and Au conventional electrode, b) the Electric field in 1D and c) in 3D with maximum levels at the Spiro-MeOTAD/Perovskite and at Perovskite/TiO_2.

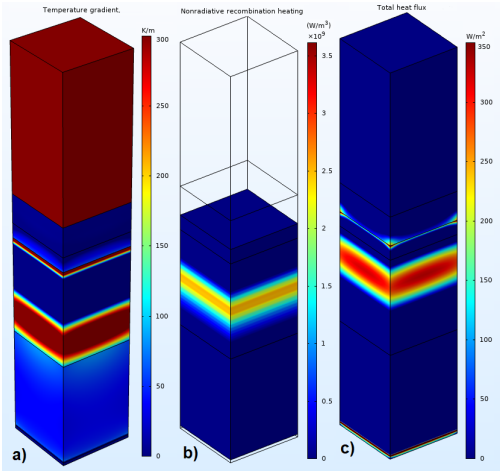


Figure 5: Thermal simulation results presenting a) Temperature gradient, b) non-radiative recombination heat, c) total heat flux including the joule heat.

study (iteration), where the temperature distribution calculated in "Heat Transfer in Solids" interface is fed back into the material temperature used in the Semiconductor interface via the second "Semiconductor Material Model" node.

3.1. Optical simulations

Both 3D and 1D simulations of the generation rate of the cell under 1 sun, AM1.5 irradiation has been displayed in Fig. 3. Photo-generation rate shows a maximum at the Perovskite/TiO_2 interface and gradually decreases towards the Sprio-MeOTAD/Perovskite junction. The calculated G_{tot}= 2.5 × 10^{28} 1/cm^3.s and 0.25 × 10^{28} 1/cm^3.s at the Perovskite/TiO_2 and Spiro/Perovskite junctions, respectively. Almost a similar peak is also observed at the RGO/Spiro contact because a Schottky contact is formed at this junction and a higher photo-generation rate is obtained [25]. The photogenreation map is in agreement with the simulation results presented in literature [26, 27] where the generation rate was reported in the order of 10^{27} for Au contacted perovskite cell. In our model we have used the following photogenration equation [28],

$$G_{opt}(\lambda) = \frac{\epsilon^{\text{“}}|E|^2}{2\hbar}, \tag{1}$$

where $\epsilon^{\text{“}}$ and E are the imaginary part of the dielectric and the electric field distribution, respectively. The photogeneration can be validated by extended form given in Ref. [25],

$$G(\lambda, x) = \eta_0 \frac{P\lambda}{hc} \alpha e^{-\alpha x}, \tag{2}$$

where, h and c are the Planck's constant and light velocity, λ is the wavelength, P is a measure of reflection, transmittance and optical-loss for every wavelength, α is absorption coefficient, x is the distance, η_0 is internal carrier collection quantum efficiency. The generation rate of different designs of perovskite solar cells has also been simulated using COMSOL and presented in literature. Abdelraouf et al. have calculated a range of 5.8-7.46 ×10^{29} 1/cm^3.s for a planar and nanotubular structure inserted in the perovskite layer [27]. This order of magnitude for G_{tot} is also in agreement with our calculations. Conversely, Snaith group has reported a few order of magnitude smaller generation rate (10^{23}) from a modified perovskite solar cell with SnO_2 or SiO_2 deposited over the FTO contact [29].

3.2. Electrical Simulation

The electrical characteristics of the cell were also simulated using the Semiconductor module with photogeneration rate inserted from the Optical module. Note that we enabled the Trap associated recombination in the semiconductor module. The current density- voltage (JV) curve of the RGO-contacted cell has been extracted and compared with the Au contacted cell [17] and given in Fig. 4a. There is a little downshift in the JV characteristics of the RGO-contacted cell which is consistent with the experimentally reported results for such a hybrid cells [30, 31]. The reason of such a deficit is usually attributed to incomplete carrier collection from the RGO-electrode due to a mismatch between the graphene orbitals and the plane perovskite lattice [16].

Fig. 4 displays the electric field distribution in 1D and 3D at open-circuit voltage resulted by solving the Poisson's equation. The nonuniform electric field is formed across the structure with a couple of peaks at the interface of Perovskite/TiO_2 and Perovskite/Spiro caused by high charge densities in the doped regions.

3.3. Thermal simulation

We must also explore the effect of heating due to optical absorption on the electrical performance of the solar cell

under normal mode of operation [19]. The photovoltaic devices are not just the optical and electrical systems, but also typical thermodynamic systems; these three physical domains are tightly coupled. To realize how the performance of a solar cell fluctuates over time, we must go through a coupled optical, thermal, drift-diffusion an ion reaction (kinetics) physics and solve the coupled model using a time-dependent solver. A correct formulation of this problem will have to take into account the heat generation and conduction, through carrier generation, transport and the interactions between electrons, holes, and host lattice. Thus, the heat flux, heat distribution, temperature map must be tightly coupled with the carrier transport (their electrical behavior). To obtain an insight into the heat distribution in a cell structure and the temperature gradient in every layer, we performed the thermal simulations by coupling the thermal module to semiconductor and optic modules. Great analytical models have been presented in literature for thermodynamic behavior of physical devices [32] and solar cells (heat generation and conduction) [33]. The general heat equation is given by PDE and must be solved in steady-state is as follows for a solid body,

$$-k\nabla^2 T + Q = \rho_p C_p \frac{dT}{dt} \tag{3}$$

where k, C_p and ρ_d are the thermal conductivity of the material as a function of temperature [W/(m.K)], the specific heat [J/(kg.K)], and the density at constant pressure, respectively. Q is a source term that controls the net energy absorbed at the sample surface from the side exposed to the concentrated solar radiation. It has been assumed that the concentrated radiation was uniformly distributed on the cell surface from air in the given cell schematic. Heat transfer on the upper graphene side occurred by natural convection and surface radiation. Usually, a linear radiative-convective transfer coefficient, h, is introduced to model the heat transfer between the top and side surfaces and the ambient at temperature T_{ext}, as described by equation [34],

$$-n(-k\nabla T) = h(T_{ext} - T). \tag{4}$$

Using the thermal parameters of all the layers including RGO, we have simulated the temperature distribution across the cell as shown in Fig. 5. The temperature distribution (Fig. 5a) is showing that the bottom layer (RGO) is less hot than the other layers which are also reasonable since the contact acts as a heat sink and a greater conductor with a higher area close to the air environment. The latter fosters the heat dissipation from its surface thus it will remain cooler than the other layers. Instead, the temperature at the junction of perovskite and TiO_2 is higher since their heat coefficient is an order of magnitude different (10^6 vs. 10^2 W/m^2.K). It's noted that this temperature map is for a steady-state calculation and the dynamic change of the temperature must be still considered through an iteration for a time-dependent calculation. The non-radiative

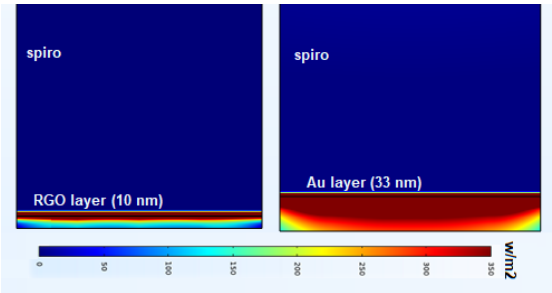


Figure 6: Heat distribution at the bottom side of the cell: a) RGO/Spiro junction and b) Au/Sprio contact.

recombination across the cell will also heat up the cell as we stated in our previous paper [17]. This heating reaches it's maximum at the middle of the perovskite layer which is expected since the SRH recombination is maximum at this area. The non-radiative recombination at RGO/Spiro interface is not significant since we assumed a minimum of 10^6 cm/s for the surface recombination velocity which limits the recombination within the mid-gap defect or traps at this interface.

The total heat flux is showing an interesting feature with three maximum at perovskite/TiO_2, perovskite bulk and RGO/Spiro areas. Each maximum is related to it's previous source e.g. SRH recombination heat and Joule heat. At the RGO/Spiro junction, the heat flux reaches a maximum also because the heat coefficient is not uniform but with three orders of magnitude difference. In this situation, heat will be accumulated at the interface near the spiro layer and the flow of heat would be slow. However, the thin RGO layer with high thermal conductivity will foster the heat dissipation and thus we see a small heat accumulation area at this interface.

In order to show the quality of heat dissipation at the RGO/spiro interface, we have drawn our comparison for two cells with RGO and Au contacts as shown in Fig. 6. A great difference is observed between the tow configuration. RGO/spiro shows minimum heat accumulation with most areas being colder and just a thin heated area near the junction. Instead, the Au conventional layer is heated and just at the corners we see a colder area. A greater heat dissipation is shown for RGO electrode.

4. Conclusion

Our 3D simulation results combined with the models presented in semi-classical approaches in literature and the experimental data provide valuable guidelines for designing efficient and stable perovskite solar cells. Graphene derivations are promissing replacement for conventional metallic electrodes e.g. for a bifacial perovskite solar cell where graphene layer can be used for both top and bottom electrodes. We have solved a coupled optical-electrical-thermal model using COMSOL multiphysics simulation

package. The results suggest that although the electrical characteristics of the cell are slightly down-shifted with graphene, the thermal trends of the cell improved due to a high thermal conduction and thin thickness of RGO layer. The heat flux shows a reduced gradient at the RGO/spiro interface resulted from accelerated heat dissipation in such a hybrid junction. The total heat flux made of Joule heat, SRH non-radiative heat and radiative heat is also showing an improved heat distribution since the high conductivity of RGO at the bottom is accelerating the heat dissipation, which in turn, prevents the heat accumulation at the interfaces or within the bulk of the cell. The thermal redistribution across the cell promotes the cell thermal stability since the solar cell's behavior is dependent on heat generation and dissipation in the cell via kT terms in Stephan-Boltzmann's approximations.

References

[1] R. Hu, L. Chu, J. Zhang, X. Li, W. Huang, ''carbon materials for enhancing charge transport in the advancements of perovskite solar cells", *Journal of Power Sources*, 361 (2017) 259-275.

[2] S. Rafique, N.A. Roslan, Sh.M. Abdullah, L. Li, A. Supangat, A. Jilani, M. Iwamoto, ''UV- ozone treated graphene oxide/ PEDOT:PSS bilayer as a novel hole transport layer in highly efficient and stable organic solar cells", *Organic Electronics*, 66 (2019) 32-42.

[3] T H. Chowdhury, Md. Akhtaruzzaman, Md. E. Kayesh, R. Kaneko, T. Noda, J.J. Lee, A. Islam, ''Low temperature processed inverted planar perovskite solar cells by r-GO/CuSCN hole-transport bilayer with improved stability", *Solar Energy*, 171 (2018) 652-657.

[4] S. Schöche, N. Hong, M. Khorasaninejad, A. Ambrosio, E. Orabona, P. Maddalena, F. Capasso, ''Optical properties of graphene oxide and reduced graphene oxide determined by spectroscopic ellipsometry", *Applied Surface Science*, 421 (2017) 778-782.

[5] D. Li, J. Cui, H. Li, D. Huang, M. Wang, Y. Shen, ''Graphene oxide modified hole transport layer for $CH_3NH_3PbI_3$ planar heterojunction solar cells", *Solar Energy*, 131 (2016) 176-182.

[6] A. L.Palma, L. Cinà, S. Pescetelli, A. Agresti, M. Raggio, R. Paolesse, F. Bonaccorso, A. DiCarlo, ''Reduced graphene oxide as efficient and stable hole transporting material in mesoscopic perovskite solar cells",*Nano Energy*, 22 (2016) 349-360.

[7] B. M. Soucase, I. G. Pradas, K. R. Adhikari, "Numerical Simulations on Perovskite Photovoltaic Devices", Book Chapter (15): Perovskite Materials - Synthesis, Characterisation, Properties, and Applications, *InTech. open science Publications*, (2016) pp. 445-490.

[8] X. Wu, P. Liu, L. Ma, Q. Zhou, Y. Chen, J. Lu, S. Yang, ''Two-dimensional modeling of TiO_2 nanowire based organic-inorganic hybrid perovskite solar cells", *Solar Energy Materials & Solar Cells*, 152 (2016) 111-117.

[9] B. Lavery S. Kumari, H. Konermann, G. L. Draper, J. Spurgeon, T. Druffel, ''Intense Pulsed Light Sintering of $CH_3NH_3PbI_3$ Solar Cells", *ACS Appl. Mater. Interfaces*, 8 (2016) 8419-8426.

[10] A. K. Kang, M. H. Zandi, N.E. Gorji, ''Simulation analysis of graphene contacted perovskite solar cells using SCAPS-1D", *Optical and Quantum Electronics*, 51 (2019) 91-100.

[11] A. Zhang, Y. Chen, J. Yan, ''Optimal Design and Simulation of High-Performance Organic-Metal Halide Perovskite Solar Cells", *IEEE Journal Of Quantum Electronic* 52:6 (2016) 1600106.

[12] Y. Shao, J. J. Yang, M. Huang, "A Review of Computational Electromagnetic Methods for Graphene Modeling", *International J. of Antennas & Propagation*, 7478621 (2019).

[13] F.Y. Niyat, M. H. Sh. Abadi, "COMSOL-Based Modeling and Simulation of SnO_2/rGO Gas Sensor for Detection of NO_2", *Scientific Reports*, 8 (2018) 2149.

[14] P. Paletti, R. Pawar, G. Ulisse, F. Brunetti, G. Iannaccone, G. Fiori, ''Can graphene outperform indium tin oxide as transparent electrode in organic solar cells?", *2D Materials*, 2 (2015) 045006.

[15] https://www.comsol.com/blogs/the-graphene-revolution-part-2/.

[16] J. Boucle, N. Herlin-Boime, ''The benefits of graphene for hybrid perovskite solar cells", *Synthetic Metals*, 222 (2016) 3-16.

[17] A. K. Kang, M.H. Zandi, N. E. Gorji, "Simulation analysis of graphene contacted perovskite solar cells using SCAPS-1D", *Optical and Quantum Electronics*, 51(4) (2019) 91.

[18] V.W. Brar, M. S. Jang, M. Sherrott, J. J. Lopez, H.A. Atwater, "Highly confined tunable mid-infrared plasmonics in graphene nanoresonators," *Nano Letters*, 13:6,2013 . 2541–2547, .

[19] Shang A, Li X. ''Photovoltaic Devices: Opto-Electro-Thermal Physics and Modeling", *J. of Advanced Materials* 2016.

[20] F. Ma, H. B. Zheng, Y. J. Sun, D. Yang, K. W. Xu, P. K. Chu, ''Strain effect on lattice vibration, heat capacity, and thermal conductivity of graphene", *Appl. Phys. Lett.*, 101 (2012) 111904.

[21] Y. Zeng, T. Li, Y. Yao, T. Li, L. Hu, A. Marconnet, "Thermally Conductive Reduced Graphene Oxide Thin Films for Extreme Temperature Sensors", *Adv. Funct. Mater.*, 29 (2019) 1901388.

[22] S. Wenger, M. Schmid, G. Rothenberger, A. Gentsch, M. Grätzel, J. O. Schumacher, "Coupled optical and electronic modeling of dye-sensitized solar cells for steady-state parameter extraction." *The Journal of Physical Chemistry C*, 115:20 (2011) 10218-10229.

[23] J.M. Ball, S. D. Stranks, M.T. Hörantner, S. Hüttner, W. Zhang, E. J. Crossland, H. J. Snaith, "Optical properties and limiting photocurrent of thin-film perovskite solar cells", *Energy & Environmental Science*, 8:2 (2015) 602-609

[24] Sh. Huang, J. Bao, H. Ye, N. Wang, G. Yuan, Y. Fu, L. Ye, K. Jeppson, J. Liu, ''The Effects of Graphene-Based Films as Heat Spreaders for Thermal Management in Electronic Packaging", 17^{th} *Intnl. Conf. on Electronic Packaging Tech.*, (2016) 16357515

[25] Z. A. Ansari, Th. J. Singh, Sk. M. Islam, et al. ''Photovoltaic solar cells based on graphene/gallium arsenide Schottky junction", *Optik*, 182 (2019) 500-506.

[26] S. Zandi, M. Razaghi, "Finite element simulation of perovskite solar cell: A study on efficiency improvement based on structural and material modification", *Solar Energy*, 179 (2019) 298-306.

[27] O. A.M. Abdelraouf, N. K. Allam, "Towards nanostructured perovskite solar cells with enhanced efficiency: Coupled optical and electrical modeling", *Solar Energy*, 137 (2016) 364-370.

[28] M. G. Deceglie, V. E. Ferry, A. P. Alivisatos, H. A. Atwater, "Design of Nanostructured Solar Cells Using Coupled Optical and Electrical Modeling", *Nano Lett.*, 12 (2012) 2894-2900.

[29] J. M. Ball, S. D. Stranks, M. T. Hörantner, S. Hüttner, W. Zhang, E. J. W. Crossland, I. Ramirez, M. Riede, M. B. Johnston, R. H. Friend, H. J. Snaith, "Optical properties and limiting photocurrent of thin-film perovskite solar cells", *Energy & Environmental Science*, 8 (2015) 602-609.

[30] G. Kakavelakis, T. Maksudov, G. Kioseoglou, E. Stratakis, E. Kymakis''Efficient and Highly Air Stable Planar Inverted Perovskite Solar Cells with Reduced Graphene Oxide Doped PCBM Electron Transporting Layer", *Adv. Energy Mater.*, 7 (2017) 1602120.

[31] P. You , Zh. Liu, Q. Tai, Sh. Liu, F. Yan, "efficient semitransparent perovskite solar cells with graphene electrodes", *Adv. Mater.*, 27:24 (2015) 1-7.

[32] W. Rellam, A. Aissat, H. Bougerir, S. Nacer, "Modelling a buried double junction photodetector using COMSOL", *Optik*, 126 (2015) 4046-4049.

[33] M. D. Perez, N. E. Gorji, ''Modeling of temperature profi le, thermal runaway and hot spot in thin fi lm solar cells", *Materials Science in Semiconductor Processing*, 41 (2016) 529-534.

[34] S. Subrina, D. Kotchetkov, "Simulation of Heat Conduction in Suspended Graphene Flakes of Variable Shapes", *Journal of Nanoelectronics and Optoelectronics*, 3 (2008) 1-21.



https://dspace.org/

Numerical simulation of heat distribution in RGO-contacted perovskite solar cells using COMSOL

Zandi, Soma; Saxena, Prateek; Gorji, Nima E.

2020-01-06
Elsevier
https://doi.org/10.1016/j.solener.2019.12.050
Zandi S, Saxena P, Gorji NE. (2020) Numerical simulation of heat distribution in RGO-contacted perovskite solar cells using COMSOL. Solar Energy, Volume 197, February 2020, pp. 105-110

Downloaded from a DSpace repository. https://dspace.org/